

Non-line-of-sight identification in ultra-wideband systems based on received signal statistics

S. Venkatesh and R.M. Buehrer

Abstract: Non-line-of-sight (NLOS) propagation can severely degrade the reliability of communication and localisation accuracy in indoor ultra-wideband (UWB) 'location-aware' networks. Link adaptation and NLOS bias mitigation techniques have respectively been proposed to alleviate these effects, but implicitly rely on the ability to accurately distinguish between LOS and NLOS propagation scenarios. A statistical NLOS identification technique based on the hypothesis-testing of received signal parameters in UWB propagation channels is discussed. In contrast to narrowband and wideband signals, UWB signals possess higher temporal resolution and robustness to multipath fading. We show that these characteristics result in differences in the statistics of (a) the time-of-arrival (TOA), (b) the received signal strength (RSS) and (c) the root-mean-squared delay spread (RDS) of the received signals, between LOS and NLOS propagation scenarios, which can be exploited for accurate channel identification. We statistically characterise the ability of TOA, RSS and RDS estimates to distinguish between LOS and NLOS propagation based on an extensive indoor measurement campaign. Our measurement results suggest that the RDS of UWB signals can, even in isolation and without complete statistical information, serve as a robust and computationally efficient indicator of the LOS/NLOS nature of propagation. Finally, we demonstrate the efficacy of the discussed NLOS identification method in a location-tracking application based on indoor UWB measurements.

1 Introduction

Impulse-based ultra-wideband (UWB) or impulse-radio [1] is expected to achieve increased commercial use in the near future [2], because of its robustness in harsh multipath environments, its ability to combine accurate ranging and localisation with low data-rate communication [3, 4] and its covertness for tactical applications. The majority of applications envisioned for impulse-radio networks leverage the fusion of communications, sensing and localisation capabilities, particularly in *indoor* scenarios. In such networks, since the line-of-sight (LOS) path between nodes may be obstructed or severely attenuated, (a) communication-link quality can be significantly degraded, and (b) range estimates based on time-of-arrival (TOA) or received signal strength (RSS) are biased with high probability [5]. These effects result in the overall degradation of both reliability of communication and localisation accuracy [6] in non-line-of-sight (NLOS) scenarios.

In order to alleviate the effects of NLOS propagation on communication link quality and localisation accuracy, link adaptation [7] and NLOS bias mitigation techniques (see [5, 8], and the references therein) have, respectively, been suggested. It has been shown that [8, 9] NLOS range estimates can be utilised to *improve* localisation accuracy, despite the presence of bias errors. However, such techniques implicitly rely on the ability to distinguish between LOS and NLOS propagation channels. Statistical NLOS

identification techniques for cellular systems have been discussed previously [6, 10] that rely on a time-series of range measurements. A comprehensive discussion of a decision-theoretic framework for NLOS identification based on the statistical distributions of range estimates in LOS and NLOS scenarios was presented in [10].

Although such approaches [6, 10], can be directly extended to UWB networks, (i) for mobile location-aware networks, using a time-series of range estimates may not be feasible, and (ii) specific features of UWB multipath channels can be exploited to enhance the accuracy of NLOS identification. In particular, UWB signals possess higher temporal resolution and robustness to multipath fading than narrowband and wideband signals. These characteristics create considerable differences in the behaviour of (a) the TOA, (b) RSS and (c) the temporal energy dispersion of the received signal in different propagation scenarios. The temporal dispersion of received signal energy in indoor UWB propagation channels has been extensively characterised (see, for instance, [11, 12]), and is quantified through the delay-spread statistics, such as the root-mean-squared delay spread (RDS) [11].

We formulate a NLOS identification technique based on the joint statistical hypothesis testing of a *single set* of TOA, RSS and RDS estimates from a given received UWB signal. We initially assume that the statistical models for the TOA, RSS and RDS estimates are known a priori from a statistical characterisation of the propagation environment. Since the distributions of these parameters are known to vary with the distance [11, 12], between the transmit and receive nodes, the distance is modelled as a nuisance parameter that needs to be estimated. Given a distance estimate, we show that combinations of conditional probabilities of the estimated values of the TOA, RSS and RDS can provide reliable estimates of the state of the channel (LOS or NLOS).

We show that for the channel parameters extracted from the UWB measurements discussed in [11], the use of RDS estimates provides the most accurate means of identifying the channel state, with a probability of error on the order of 1%. Further, we show that delay-spread statistics of the received signal remain a reliable means of channel state identification when (a) the complete statistical characterisation of the propagation environment is unknown a priori, and (b) when an accurate estimate of the distance is not available. Performance metrics that allow the evaluation of the proposed techniques in other propagation scenarios with different statistical models are provided. Finally, the performance of the NLOS identification based on delay-spread statistics, from the perspective of localisation accuracy, is investigated in a location-tracking experiment with indoor UWB measurements.

This paper is organised as follows: in Section 2, we discuss the modelling of the statistics of the TOA, RSS and RDS estimates in indoor LOS and NLOS environments based on the UWB measurement campaign discussed in [11]. The formulation of the statistical hypothesis-testing method is outlined in Section 3, and the corresponding simulation results are presented in Section 4. The performance of hypothesis-testing of delay-spread statistics using actual measurement results is presented in Section 5. We draw conclusions in Section 6.

2 Statistics of the UWB TOA, RSS and RDS estimates in indoor environments

The formulation of the NLOS identification problem is as follows: we would like to identify the state H of the channel between the transmit and receive nodes, separated physically by a distance d , given estimates of the TOA, RSS and RDS observed at the receive node. Here, the channel state $H = H_0$ corresponds to LOS propagation and $H = H_1$ corresponds to NLOS propagation. NLOS propagation has popularly been classified as ‘soft’ (‘obstructed’) NLOS, where the LOS multipath component is present albeit attenuated, and ‘hard’ NLOS, where the LOS path is severely attenuated or absent. From a localisation standpoint, the soft-NLOS cases are classified as LOS scenarios, since the TOA of the LOS multipath component can still be estimated for ranging purposes, that is, range estimates are not necessarily biased in soft-NLOS propagation environments. In the following development, we present statistical models for the TOA, RSS and RDS estimates in an indoor UWB channel, considering both LOS and NLOS scenarios.

2.1 TOA estimates

The received UWB signal, neglecting non-linear effects, can be modelled as a function of time τ :

$$r(\tau) = \sum_{k=0}^{L-1} \alpha_k p(\tau - \tau_k) + n(\tau)$$

where $p(\tau)$ is the received (LOS) pulse shape, α_k , $k = 0, 1, \dots, L-1$ denote the L multipath coefficients, and $n(\tau)$ represents additive white Gaussian noise at the receiver. Here, $\tau_0 = d/c$ represents the true TOA of the signal, where c denotes the speed of light. In LOS propagation conditions, the estimate of the TOA $\hat{\tau}_0$ is modeled as [3, 13] an unbiased Gaussian random variable

$$\hat{\tau}_0 = \frac{d}{c} + n_\tau \quad (H = H_0)$$

where n_τ is the zero-mean Gaussian TOA measurement noise. The corresponding density function of $\hat{\tau}_0$, conditioned on the distance d is then given by

$$f_{\hat{\tau}_0}(\tau|d, H_0) = (2\pi\sigma_\tau^2)^{-1/2} \exp\left(-\frac{(\tau - (d/c))^2}{2\sigma_\tau^2}\right)$$

where σ_τ represents the standard deviation of the TOA measurement noise. Since the minimum variance of an unbiased TOA estimate is known to be inversely proportional to the signal-to-noise ratio [14], the standard deviation of the TOA estimates σ_τ is dependent on the distance d , and is modeled as:

$$\sigma_\tau = K_\tau d^{\beta/2}$$

where K_τ is a proportionality constant that depends on physical layer parameters, and β is the path-loss exponent.

In a NLOS propagation scenario, the multipath component corresponding to the true distance d between the nodes is either absent or severely attenuated, and the TOA estimate $\hat{\tau}_0$ is positively biased with high probability. The model for $\hat{\tau}_0$ in NLOS conditions is therefore the superposition of an unbiased Gaussian measurement noise and a random positive bias

$$\hat{\tau}_0 = \frac{d}{c} + n_\tau + b_\tau \quad (H = H_1)$$

where b_τ is the NLOS bias. The NLOS bias b_τ is assumed to be independent of the range measurement noise and has been modelled as an exponential random variable [13] with mean λ_b . Based on these assumptions, as shown in Appendix 1, the density function of $\hat{\tau}_0$, conditioned on the distance d , can be written as

$$f_{\hat{\tau}_0}(\tau|d, H_1) = \frac{1}{2\lambda_b} \exp\left(\frac{\sigma_\tau^2}{2\lambda_b^2}\right) \exp\left(-\frac{(\tau - (d/c))}{\lambda_b}\right) \times \left[1 + \operatorname{erf}\left(\frac{\lambda_b(\tau - (d/c)) - \sigma_\tau^2}{\sqrt{2}\sigma_\tau\lambda_b}\right)\right]$$

Summarising the above results, the density functions of the TOA estimate $\hat{\tau}_0$ for the two propagation scenarios can be written as

$$f_{\hat{\tau}_0}(\tau|d, H) = \begin{cases} (2\pi\sigma_\tau^2)^{-1/2} \exp\left(-\frac{(\tau - (d/c))^2}{2\sigma_\tau^2}\right), & H = H_0 \\ \frac{1}{2\lambda_b} \exp\left(\frac{\sigma_\tau^2}{2\lambda_b^2}\right) \exp\left(-\frac{(\tau - (d/c))}{\lambda_b}\right) \left[1 + \operatorname{erf}\left(\frac{\lambda_b(\tau - (d/c)) - \sigma_\tau^2}{\sqrt{2}\sigma_\tau\lambda_b}\right)\right], & H = H_1 \end{cases} \quad (1)$$

In the above equations

$$\sigma_\tau = \begin{cases} K_\tau d^{\beta_L/2}, & H = H_0 \\ K_\tau d^{\beta_N/2}, & H = H_1 \end{cases}$$

where β_L and β_N represent the path-loss exponents in LOS and NLOS scenarios, respectively.

2.2 RSS estimates

The normalised RSS (in dB) S_{dB} is defined as

$$S_{\text{dB}} = 10 \log_{10} \left(\frac{1}{P_0 T} \int_T |r(\tau)|^2 d\tau \right)$$

where P_0 is the received power measured at a reference distance d_0 , and T is the measurement interval for the received signal. Because of the absence of significant multipath fading, the estimated RSS has been modelled as a lognormal random variable [11, 12, 15]

$$\hat{S}_{\text{dB}} = 10\beta \log_{10}\left(\frac{d}{d_0}\right) + X$$

where β is the path loss exponent, and X is a zero-mean Gaussian random variable with different variances in LOS and NLOS scenarios

$$f_X(x) = \begin{cases} (2\pi\sigma_{SL}^2)^{-1/2} \exp\left(-\frac{x^2}{2\sigma_{SL}^2}\right), & H = H_0 \\ (2\pi\sigma_{SN}^2)^{-1/2} \exp\left(-\frac{x^2}{2\sigma_{SN}^2}\right), & H = H_1 \end{cases}$$

Therefore in LOS and NLOS scenarios, the conditional density functions of \hat{S}_{dB} can be succinctly represented by

$$f_{\hat{S}_{\text{dB}}}(s|d, H) = \begin{cases} (2\pi\sigma_{SL}^2)^{-1/2} \exp\left(-\frac{(s - 10\beta_L \log_{10}(d))^2}{2\sigma_{SL}^2}\right) & H = H_0 \\ (2\pi\sigma_{SN}^2)^{-1/2} \exp\left(-\frac{(s - 10\beta_N \log_{10}(d))^2}{2\sigma_{SN}^2}\right) & H = H_1 \end{cases} \quad (2)$$

2.3 RDS estimates

Given the received signal $r(\tau)$, and the received LOS pulse $p(\tau)$, the temporal channel impulse response $h_c(\tau)$ can be estimated using a deconvolution algorithm such as the CLEAN algorithm [16], which has previously been applied to impulse-based UWB measurements [16, 17]. The estimated channel impulse response $\hat{h}_c(\tau)$ is a superposition of \hat{L} discrete multipath components

$$\hat{h}_c(\tau) = \sum_{k=0}^{\hat{L}-1} \hat{\alpha}_k \delta(\tau - \hat{\tau}_k) \quad (3)$$

where $\hat{\alpha}_k$ and $\hat{\tau}_k$ are the estimated amplitude (including polarity) and arrival-time of the k -th multipath component, respectively. The estimated number of multipath components \hat{L} is determined by the relative strengths of the multipath components and the amplitude threshold applied by the deconvolution algorithm. The deconvolution algorithm typically retains those multipath components whose amplitudes are within a certain threshold of the strongest multipath component. The most common metric used to quantify the dispersion of the received signal energy over time by the channel is the RDS $\hat{\tau}_{\text{rms}}$, which is defined as

$$\hat{\tau}_{\text{rms}} = \sqrt{\frac{\sum_k \hat{\alpha}_k^2 \hat{\tau}_k^2}{\sum_k \hat{\alpha}_k^2} - \hat{\tau}_m^2} \quad (4)$$

where $\hat{\tau}_m$ is the mean excess delay of the channel, defined as $\hat{\tau}_m = \sum_k \hat{\alpha}_k^2 \hat{\tau}_k / \sum_k \hat{\alpha}_k^2$. Fig. 1 illustrates the dispersion in the received multipath energy over time in two sample LOS and NLOS channel measurements [11]. In the LOS case, the energy is seen to be concentrated in the first-arriving path, whereas in the NLOS case, the energy is well distributed over several multipath components. We see that this difference is captured by the values of $\hat{\tau}_{\text{rms}}$ computed for the two cases. Further, we also observe that for a

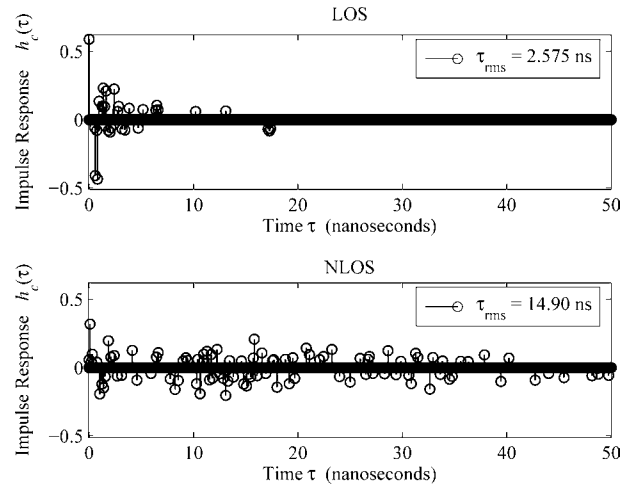


Fig. 1 Sample LOS (top) and NLOS (bottom) channel impulse responses in an indoor office propagation measurement [11]

Both channel impulse responses were computed using the CLEAN algorithm with a threshold of 20 dB, and were subsequently normalised to unit energy. The RMS delay spread and the number of significant multipath components in the LOS and NLOS cases are, respectively, 2.575 ns and 25 (top), and 14.90 ns and 76 (bottom)

fixed amplitude threshold (20 dB in this case), the estimated number of multipath components \hat{L} is much larger in the NLOS case than the LOS case.

The RDS estimate has been observed to be positive and Gaussian distributed in several measurement campaigns [11, 12, 15]. Further, it has been observed [11, 12, 15, 18] that the average RDS increases with the distance between the nodes. The rationale behind this trend is that the average number of significant scatterers in a typical indoor propagation environment increases as the distance between the transmit and receive antennas increases. The mean of the RDS estimate (in nanoseconds) is assumed to increase linearly with distance [11, 12, 18] as

$$\mu_{\hat{\tau}_{\text{rms}}}(d) = \begin{cases} a_L(d - d_0) + b_L, & H = H_0 \\ a_N(d - d_0) + b_N, & H = H_1 \end{cases}$$

and we assume that the variance of the RDS estimates $\sigma_{\hat{\tau}_{\text{rms}}}^2$ is independent of distance. With these assumptions, the distribution of the RDS estimate can be written as

$$f_{\hat{\tau}_{\text{rms}}}(\tau, d|H) = \begin{cases} c_L (2\pi\sigma_{\hat{\tau}_{\text{rms},L}}^2)^{-1/2} \exp\left(-\frac{(\tau - (a_L(d - d_0) + b_L))^2}{2\sigma_{\hat{\tau}_{\text{rms},L}}^2}\right) u(\tau), & H = H_0 \\ c_N (2\pi\sigma_{\hat{\tau}_{\text{rms},N}}^2)^{-1/2} \exp\left(-\frac{(\tau - (a_N(d - d_0) + b_N))^2}{2\sigma_{\hat{\tau}_{\text{rms},N}}^2}\right) u(\tau), & H = H_1 \end{cases} \quad (5)$$

where $u(\cdot)$ is the Heaviside function, and $\{c_L, c_N\}$ are normalisation constants that ensure that the area under the above probability density functions is unity (see Appendix 2).

The parameters corresponding to the above models for the TOA, RSS and RDS estimates extracted from the measurements in [11] are presented in Table 1. In the following section, we discuss a statistical NLOS identification method based on the conditional distributions of the TOA, RSS and RDS estimates given in (1), (2) and (5), respectively.

Table 1: Parameters obtained from UWB measurements [11]

Measurement parameters	LOS $H = H_0$	NLOS $H = H_1$
β	1.8	2.5
λ_b	–	4.5 ns
σ_S	2.75	4.1
a	1.42	15.30
b	0.03	0.15
$\sigma_{\tau_{rms}}$	2.17	2.41

3 Statistical NLOS identification

Suppose we are given a set of the TOA, the RSS and the RDS estimates: $\mathcal{S} = \{x_1, x_2, x_3\}$, where x_1, x_2 and x_3 are realisations of $\hat{\tau}_0, \hat{S}_{dB}$ and $\hat{\tau}_{rms}$, respectively, obtained from the received signal. As discussed in the previous section, the conditional distributions of the TOA, RSS and RDS estimates are functions of the distance d and the channel state H , given by (1), (2) and (5), respectively. Provided the physical distance d between the transmit and receive nodes is known exactly, the state of the channel can be identified by comparing the likelihood values for each of the estimates x_i , conditioned on the distance d , for both $H = H_0$ and $H = H_1$. This is shown in Fig. 2, where the true state of the channel is $H = H_1$, and the a posteriori distribution of the distance, conditioned on the values of the available estimates for both LOS and NLOS scenarios is shown. In this example, for the known value of d , the likelihood that the available estimates occurred because of NLOS propagation rather than LOS propagation is higher, and the maximum likelihood (ML) channel state [19] would be $\hat{H} = H_1$. Evidently, if d is known, based on the likelihood values of any of the given estimates, the ML channel state can be directly obtained from the known conditional distributions of the estimates.

In reality however, we do not know the physical distance d between the nodes. Indeed, for localisation applications, estimating the distance d accurately is a requirement, and is typically done using TOA or RSS estimates. For simplicity, we assume that the distance is estimated using the TOA

$$\hat{d} = cx_1$$

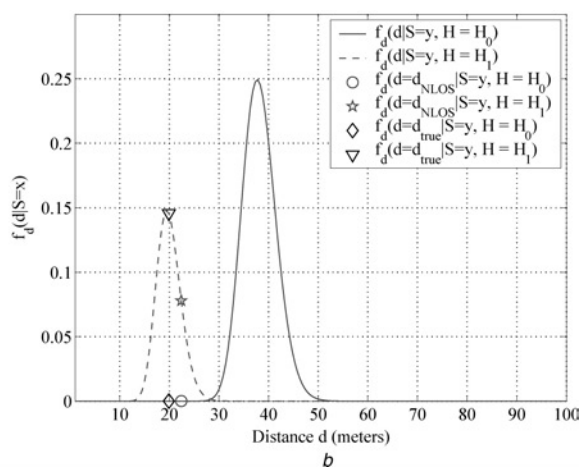
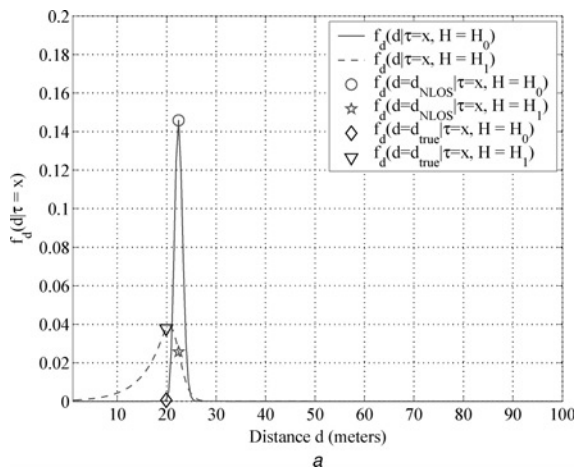


Fig. 2 A posteriori density function of the distance

a TOA estimate x and the channel state H

b RSS estimate y and the channel state H

For both plots, the true channel state is $H = H_1$

Although the above distance estimate is unbiased when $H = H_0$, it is positively biased with high probability when $H = H_1$, and therefore the likelihood of the TOA estimate cannot be used to identify the channel state as seen in Fig. 2. However, for the given RSS estimate x_2 when $H = H_1$, the probability that the received RSS estimate was obtained under NLOS propagation conditions, even with the biased distance estimate \hat{d} , is higher than the corresponding LOS probability. This suggests that joint NLOS identification based on all three estimates can improve the probability of successful identification, even with noisy and/or biased distance estimates.

The formulation of the joint channel state identification is as follows: our initial hypothesis is that the state of the channel is LOS, that is, $\hat{H} = H_0$, and that $\hat{d} = cx_1$. For each of the given estimates, we determine the conditional probabilities

$$p_i = \Pr\{X_i = x_i | \hat{d}, H_0\}$$

$$q_i = \Pr\{X_i = x_i | \hat{d}, H_1\}$$

We then compute $D_L = \prod_i p_i$ and $D_N = \prod_i q_i$. It must be pointed out that if the estimates are assumed to be independent for a fixed distance and channel state, D_L and D_N are the joint conditional probabilities of the estimates. The values of D_L and D_N can then serve as the decision metrics for estimating the channel state. In particular, if $D_N < D_L$, we change our hypothesis of the channel state from LOS to NLOS

$$\hat{H} = \begin{cases} H_0, & D_L > D_N \\ H_1, & D_L < D_N \end{cases} \quad (6)$$

After the state of the channel has been determined, the range estimate can then be updated

$$\hat{d} = \arg \max_d \Pr\{X_i = x_i | d, \hat{H}\} \quad (7)$$

which is the ML estimate of d for the given estimate x_i and the estimated channel state \hat{H} . Once the channel state and the new distance estimate have been computed, these can be fed back to verify if the conditional probabilities change, as shown in Fig. 3. The above method can be viewed as joint iterative ML estimation of the channel state, with the distance d treated as a nuisance parameter. As seen in Fig. 3, the distance d is iteratively estimated

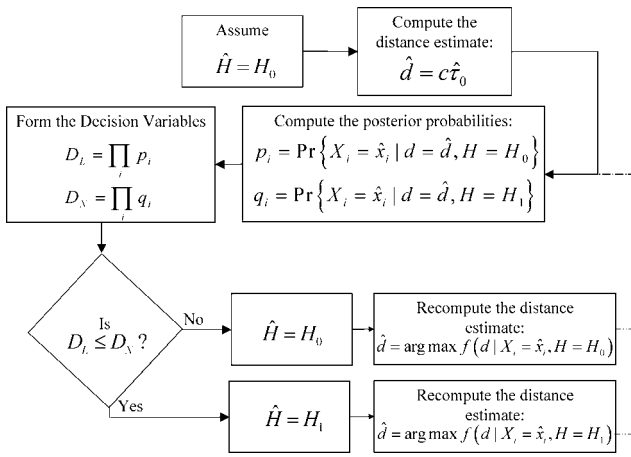
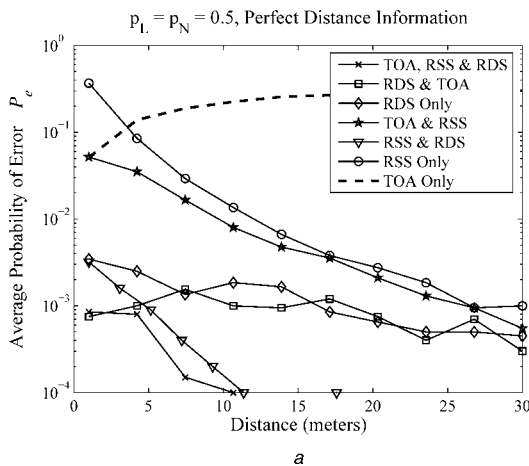


Fig. 3 Block diagram of statistical decision-theoretic framework: the joint probabilities D_L and D_N are compared to determine the channel state estimate

along with the channel state. The iteration is terminated when the estimated channel state does not change with additional iterations. It has been observed that the above iterative scheme typically converges within two iterations.

Clearly, there are variations to this scheme: we may choose to use only a subset of the estimates, depending upon their availability and/or knowledge of their statistical distributions. Specifically, in Fig. 3, to determine the decision metrics D_L and D_N , we may choose to use only TOA, or RSS, or RDS conditional probabilities, or any combination of these estimates.

In the following section, we provide simulation results that compare the efficacy of combinations of different estimates in distinguishing between LOS and NLOS propagation. We show that, based on the indoor UWB measurements in [11], the RDS estimates serve as efficient ‘differentiators’ between LOS and NLOS propagation scenarios. We further show that even in the absence of information on their statistical dependence on distance, the RDS estimates can be used through conventional hypothesis-testing to accurately identify the channel state.



4 Simulation results

The performance of decision-theoretic NLOS identification, based on the joint statistics of combinations of TOA, RSS and RDS estimates, is shown in Figs. 4a and b. There exist seven combinations of these estimates: ‘only-TOA’, ‘only-RSS’, ‘only-RDS’, ‘TOA & RSS’, ‘RSS & RDS’, ‘RDS & TOA’ and ‘TOA, RSS & RDS’. A large number of realisations of the TOA, RSS and RDS estimates are generated for each value of d between 1 and 30 m using (1), (2) and (5). A given realisation of an estimate is generated based on its corresponding conditional distribution for the LOS scenario ($H = H_0$) with probability p_L , and using the conditional distribution for the NLOS scenario ($H = H_1$) with probability $p_N = 1 - p_L$. The described hypothesis-testing approach is then applied to each realisation of the given parameters, and the channel state \hat{H} is estimated. For each value of the distance, the average probability of channel state estimation error P_e is evaluated based on the relation

$$P_e = p_L \cdot \Pr\{\hat{H} = H_1 | H = H_0\} + p_N \cdot \Pr\{\hat{H} = H_0 | H = H_1\} \quad (8)$$

In the absence of the knowledge of a priori probabilities, the channel states are assumed to be equiprobable: $p_L = \Pr\{H = H_0\} = \Pr\{H = H_1\} = p_N = 0.5$, and 10 000 realisations of the TOA, RSS and the RDS were generated for each value of d .

Fig. 4a compares the average probability of channel state estimation error P_e , when the distance between the transmit and receive nodes is known exactly, and the TOA, RSS and RDS estimates obey the statistical distributions with the parameters given in Table 1, defined in (1), (2) and (5), respectively. Given different combinations of the estimated parameters, the ML estimate of the channel state can be obtained as discussed in Section 3. Although exact distance information is typically not available, the performance of the channel state identification with perfect distance information (i) serves as an upper bound for the probability of successful identification in the case where the distance d is unknown, and (ii) helps quantify the sensitivity of the discussed channel identification techniques to the accuracy of distance estimates.

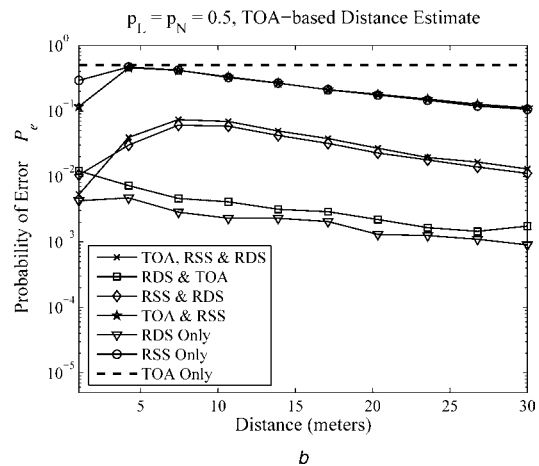


Fig. 4 Probability of error using different methods

a d is known exactly

b d is estimated using the TOA estimate

In the above simulations, it is assumed that the probability of LOS propagation is equal to the probability of NLOS propagation

Fig. 4b compares the values of P_e obtained using different combinations of the estimated parameters when d is unknown and is estimated using the iterative procedure discussed in Section 3. It must be pointed out that in all these cases, the initial distance estimate \hat{d} is obtained using the TOA estimate $\hat{\tau}_0$. It is intuitive that the ‘only-TOA’ method produces approximately 50% successful identification in Fig. 4b, as the initial hypothesis is always $\hat{H} = H_0$ and this, with high probability, results in $p_1 > q_1$. From Figs. 4a and b, we observe that although the method which uses all three estimates (‘TOA, RSS and RDS’) results in the lowest value of P_e of all the methods when perfect distance information is available (Fig. 4a), this is not the case when perfect distance information is not available (Fig. 4b). We further note that as the distance d increases, the average probability of channel state estimation error decreases, as the regions of overlap for the density functions in LOS and NLOS scenarios diminish, leading to more accurate channel state identification.

A key observation in both Figs. 4a and b is that methods incorporating the RDS estimate are most successful in differentiating between the LOS and NLOS channel states. Even in isolation, the RDS estimate can be used to distinguish between LOS and NLOS propagation conditions with a high probability of success, and adding TOA and RSS statistical information does not result in considerable gains when accurate distance information is not available. Indeed, for the statistical parameters observed in [11] and listed in Table 1, in the absence of perfect distance information, using TOA and RSS estimates in addition to the RDS estimates actually degrades the probability of successful channel state estimation, as observed in Fig. 4b.

4.1 Absence of complete statistical information

A major issue concerning the practical application of the statistical decision-theoretic method described in Section 3 is the availability of complete statistical information corresponding to received signal parameters, and particularly their variation with distance. When the conditional distributions of the received signal parameters are unknown, we may resort to ‘conventional’ hypothesis-testing, where the received signal parameter is compared with a threshold, followed by a decision on the channel state depending on whether the estimate is smaller or larger than the threshold. Because of the strong dependence of the statistics of the TOA and RSS estimates on the true distance between transmit and receive antennas, the threshold used for hypothesis-testing these estimates must be dependent on the true distance. However, as seen in Fig. 4b, the lack of perfect distance information results in considerable performance degradation when using TOA and RSS estimates with noisy and/or biased distance estimates.

On the other hand, we observed in Fig. 4b that significantly lower channel estimation error probabilities can be obtained with RDS estimates, even with noisy and biased distance estimates. Fig. 5 shows the histogram of the RDS estimates in LOS and NLOS scenarios, for all measurement distances (1–30 m) [11]. We see that regardless of d , the regions of support for the density functions of the RDS estimates remain sufficiently separated to use conventional hypothesis-testing, without requiring a distance-dependent threshold. The statistics of the RDS estimates observed in several measurement campaigns [15, 20], summarised in Table 2, indicate that the distinction between the RDS estimates in LOS and NLOS propagation scenarios is general, and not restricted to a given set of measurements. The statistics of the RDS estimates corresponding to the channel

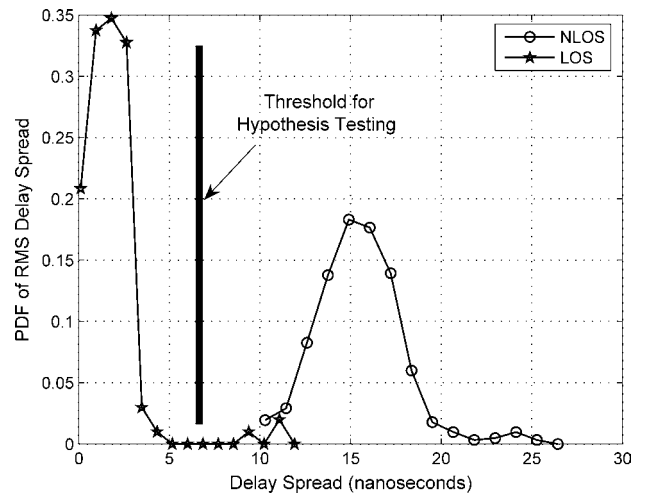


Fig. 5 Hypothesis-testing of the RMS delay spread for the nature of the UWB channel: the histogram of the RMS delay spread in LOS and NLOS scenarios for distances 1–30 m

We see that since the PDF of the RMS delay spread for the LOS and NLOS cases are well separated, the performance of NLOS identification using this approach is not sensitive to the value of the threshold selected

model adopted by the IEEE 802.15.3a subcommittee [21] are also shown. It is important to emphasise that for each of the measurement scenarios listed in Table 2, differences in the propagation environments, deconvolution algorithms and their associated parameters, types and directionality of antennas, and so on, result in the variation of the observed values of the RDS across the measurement campaigns. We would like to (a) investigate the performance of conventional hypothesis-testing of the RDS estimates for the sets of measurements listed in Table 2, and (b) quantify the extent of performance degradation because of the lack of knowledge on the statistical dependence on distance.

Table 2: RMS delay spread statistics from measurement campaigns [20]

Measurement campaign	Mean μ_L , ns	Standard deviation σ_L , ns
Indoor LOS		
AT&T [18], [23]	4.71	2.31
	3.55	1.65
Samsung/SAIT [24]	14.00	1.53
	12.87	1.87
Time domain [17]	5.27	3.37
MPRG, VT [11]	3.34	2.17
IEEE CM1 [2]	6	1.1
Indoor NLOS		
AT&T [18], [23]	8.20	3.30
	7.35	3.45
Samsung/SAIT [24]	38.61	8.03
	26.51	5.22
Time domain [17]	14.59	3.41
MPRG, VT [11]	16.08	2.41
IEEE CM2 [2]	8	0.75
IEEE CM3 [2]	14.5	2.26
IEEE CM4 [2]	25	3.7

Table 3: Computation of \mathcal{M} , P_e^* and T^* using the statistics in Table 2

Metric calculations			
Measurement campaign	Metric \mathcal{M}	Minimum probability of error P_e^*	Optimal threshold T^* , ns
AT&T (S1, S2)	0.50	0.16	6.69
	0.63	0.20	5.69
Samsung/SAIT (S3, S4)	0.14	3.5×10^{-3}	18.35
	0.23	0.024	17.1
Time domain (S5)	0.36	0.087	10.1
MPRG, VT [11] (S6)	0.18	3.3×10^{-3}	9.49
IEEE CM1-CM2 (S7)	0.43	0.13	6.97
IEEE CM1-CM3 (S8)	0.19	5.5×10^{-3}	8.86
IEEE CM1-CM4 (S9)	0.10	3.35×10^{-5}	10.76

4.2 Definition of a distance metric

Assuming that the RDS estimate is positive and Gaussian [15], as given in (5), the minimum probability of error P_e^* and the optimal threshold T^* for hypothesis-testing can be computed in a straightforward manner, as detailed in Appendix 2. In general, the values of P_e^* and T^* , respectively, given by (11) and (12), depend on the means $\{\mu_L, \mu_N\}$ and the standard deviations $\{\sigma_L, \sigma_N\}$ of the RDS estimates. In order to allow for a unified comparison of performance using different sets of measurements, we define a metric

$$\mathcal{M} = \frac{\sqrt{\sigma_L \sigma_N}}{|\mu_N - \mu_L|} \quad (9)$$

Intuitively, the metric \mathcal{M} is a measure of extent of the overlap of the probability density functions of the RDS estimates in LOS and NLOS scenarios: as \mathcal{M} decreases, P_e^* decreases. As the parameters $\{\mu_L, \mu_N, \sigma_L, \sigma_N\}$ vary, the values of the metric vary as well. However, as seen in Fig. 6, there is a strong correlation between the value of \mathcal{M} defined above and the value of P_e^* computed using (11). Further, we see that the value of P_e^* achieved largely depends on the value of \mathcal{M} , rather than the specific values of the parameters $\{\mu_L, \mu_N, \sigma_L, \sigma_N\}$.

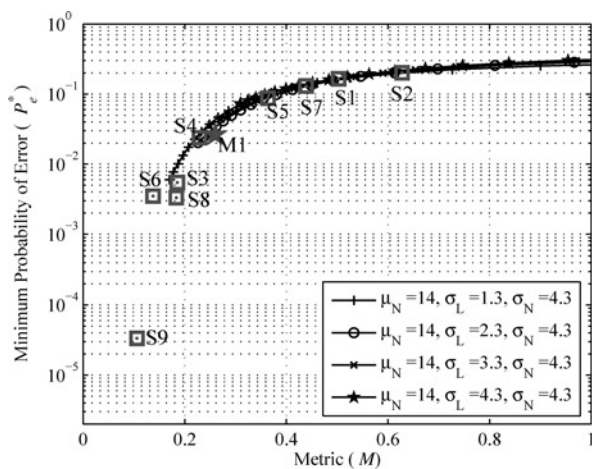


Fig. 6 Minimum probability of error P_e^* against the metric \mathcal{M} for different values of $\{\mu_L, \sigma_L, \mu_N, \sigma_N\}$

Value of μ_L is varied to obtain different values of the metric. Simulated values of P_e^* from Table 3 (S1–S9) are also shown

Table 3 lists the values of \mathcal{M} , P_e^* and T^* , respectively, computed using (9), (11) and (12) from the RDS statistics in Table 2. For each of these measurement statistics (S1–S9 in Table 2), the values of P_e^* are plotted against the values of \mathcal{M} in Fig. 6. We see that for the sets of measurements S1–S9, the probability of channel state estimation error can vary from 10^{-5} to 0.2. It must be emphasised that these values of P_e^* are obtained via simulations, under the assumption that the distribution of the RDS estimate under LOS and NLOS conditions is positive and Gaussian distributed. The direct application of the hypothesis-testing to received signal measurements over all distances [11] results in a probability of error P_e of approximately 0.02 (see (M1) in Fig. 6). With (M1), no knowledge of the distance or statistical distributions was assumed and the RDS estimates from received signal measurements were compared to a threshold $T = 9.5$ ns. This value of T was computed using the analysis in Appendix 2, and was found to provide robust performance over a large number of measurement locations. The average probability of error in scenario (M1) is about an order of magnitude larger than the ‘Only-RDS’ scenario discussed in Section 3 equipped with distance-dependent statistical knowledge, where P_e averaged over d was approximately 2×10^{-3} . Although this suggests that the lack of knowledge on the statistical dependence on distance does result in performance degradation, the performance may be acceptable for localisation applications. In the following section, we present measurement results from a location-tracking experiment that demonstrate that hypothesis-testing of the RDS estimate provides accurate channel identification from the perspective of localisation accuracy.

5 Measurement results

In order to validate the use of RDS for distinguishing between LOS and NLOS range estimates in localisation applications, a mobile tracking experiment was conducted. The schematic in Fig. 7 shows the floor plan and the measurement locations, which comprise 71 measurement points in the mobile’s trajectory and 18 anchor locations, also shown in Fig. 8a. The measurement locations in the mobile’s trajectory were separated by approximately 1.2 m. The signal received at each of these points from a

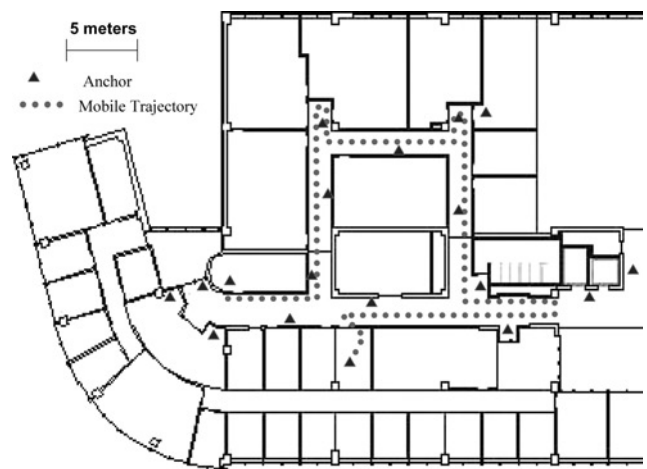


Fig. 7 Schematic of floor plan and locations of anchors and measurement points in the mobile’s ‘trajectory’

Mobile’s trajectory, represented by the dotted line, comprises 71 receiver locations, with the transmit antenna placed at one of 18 anchor locations

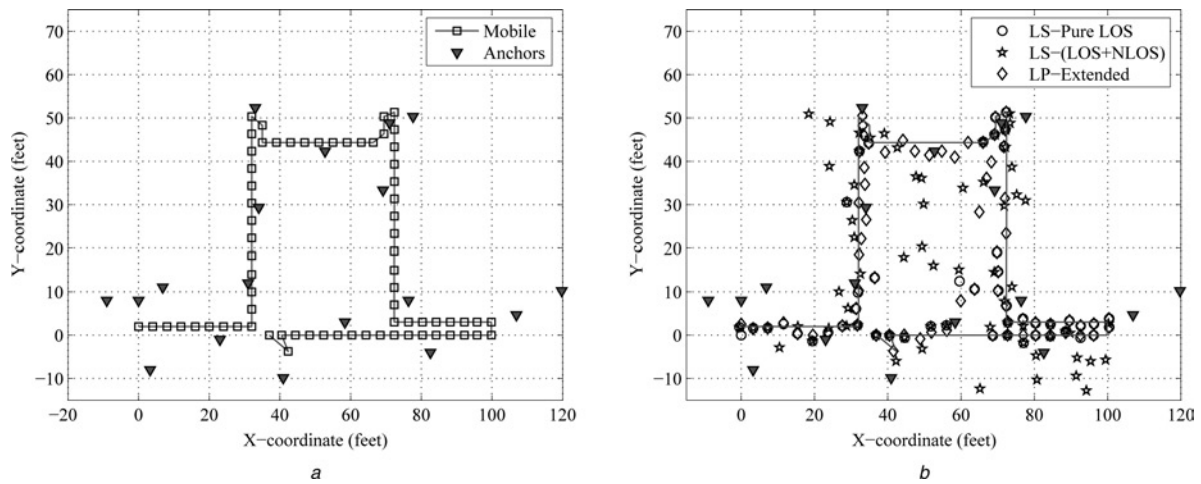


Fig. 8 Measured and estimated locations of the mobile node

a Measured locations of the mobile and anchor nodes

b Estimated locations of the mobile using the LS-(pure LOS), LS-(LOS + NLOS) and the LP-extended localisation techniques

transmitter located at different anchor locations was measured, provided the signal could be captured. A bicone antenna connected to a 30 ps pulse generator was used as the transmitter, and the receiver consisted of a second bicone antenna connected to a digital sampling oscilloscope. The received signals were subsequently bandpass-filtered with lower and upper cutoffs of 3.1 and 10.6 GHz, respectively. For each measurement location, the ‘true’ state of the channel (LOS or NLOS) was noted by observing the presence of a detectable path with a TOA corresponding to the physical distance between the antennas.

The distance between a given point in the mobile’s trajectory and a given anchor was estimated using the corresponding received signal. The range estimation algorithm was based on energy thresholding [22], and was calibrated using a reference measurement taken at a distance $d_0 = 1$ m. For each mobile measurement location, based on the range estimates obtained from the set of available anchors, the location can be estimated using a variety of methods, and compared to the physically measured location of the receive antenna. The errors arising from the physical measurement and placement of the bicone antennas are expected to be limited to within ± 10 cm.

In order to demonstrate the utility of NLOS identification in particular, and the *use* of NLOS range information in general, we compare the following localisation methods: (a) the least-squares (LS) estimator, retaining only LOS range estimates and discarding NLOS range estimates after channel state identification when more than two LOS range estimates are available (‘LS-(pure LOS)’), (b) the LS estimator incorporating all available range estimates without distinguishing between LOS and NLOS range estimates (‘LS-(LOS + NLOS)’), and (c) the linear-programming (LP) approach discussed in [8, 9], which treats LOS and NLOS range estimates differently following channel state identification (‘LP-extended’). The LS-(pure LOS) method is identical to the LS-(LOS + NLOS) method when fewer than three LOS range estimates are available. The LS-(pure LOS) method essentially represents a conservative location-estimation method where NLOS range estimates are discarded since they are known to be biased. The LS-(LOS + NLOS) method represents a ‘blind’ approach, as all range estimates, unbiased or biased, are directly incorporated into the least-squares formulation. The LP-extended method utilises LOS range estimates in a way similar to the LS-(pure LOS) method,

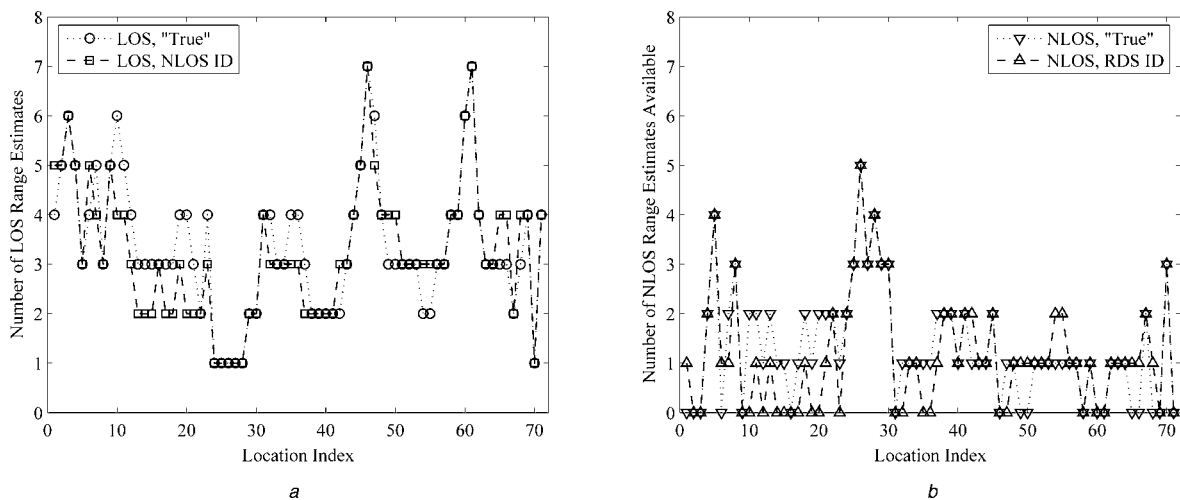


Fig. 9 Number of LOS and NLOS estimates

a LOS

b NLOS range estimates for different mobile locations observed using measurements and through channel state estimation using RMS delay-spread hypothesis-testing

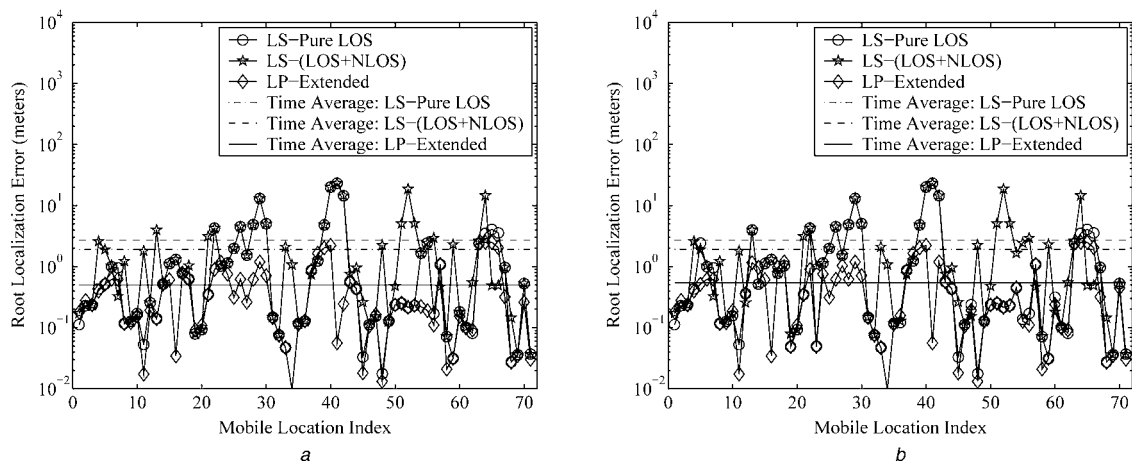


Fig. 10 Root localisation error (metres) against mobile location index obtained using different methods when

a Perfect channel state information is available

b When the channel state information is estimated from the RMS delay spread

but utilises NLOS range estimates to create a feasible region for potential solutions [8, 9], thereby resulting in the ‘soft-activation’ of NLOS range information. The three localisation methods are compared in terms of the ‘root localisation error’ (in metres), defined as the Euclidean distance between the true and estimated locations of the mobile.

Fig. 8b compares the performance of the three estimators mentioned above when channel state estimation through the hypothesis-testing of the RDS estimate is applied. A threshold $T = 9.5$ ns was used, as given in Table 3. We see that the LP-extended method outperforms both the LS-(pure LOS) and LS-(LOS + NLOS) methods in terms of localisation accuracy. Figs. 9a and b compare the number of LOS and NLOS estimates, respectively, observed during measurement and estimated using the RDS. The total probability of error P_e in channel state estimation was found to be approximately 9% using the RDS estimate. Although the results presented here correspond to hypothesis-testing of only the RDS estimate, it was verified that P_e drops to approximately 5% when both the RDS estimate and the estimated number of significant multipath components (\hat{L}) are used for hypothesis-testing.

Figs. 10a and b compare the root localisation error (in metres) achieved by the three methods, with (a) ‘perfect’ channel state information, and (b) channel state estimates based on hypothesis-testing of the RDS estimate. We see that (i) the time-averaged localisation error achieved by the LP-extended method is significantly lower than the other two methods, (ii) the use of channel state estimates based on RDS results in negligible degradation in the localisation error, when compared to the case with perfect channel state information. For instance, the performance degradation in terms of the time-averaged root localisation error for the LS-(pure LOS) and LP-extended methods are 1.4% and 5.7% respectively. We further note that after channel state identification, the time-averaged localisation error for the LS-(LOS + NLOS), LS-(pure LOS) and LP-extended methods are approximately 2.7, 1.9 and 0.5 m, respectively. This suggests that although channel state identification followed by the discarding of NLOS range estimates improves localisation accuracy, channel state identification followed by the appropriate utilisation of NLOS range estimation can provide further gains.

In summary, these measurement results indicate that (i) NLOS identification can prove beneficial, as treating the

NLOS range estimates differently from LOS range estimates can result in considerable gains in terms of localisation accuracy, and (ii) the delay-spread statistics can be used successfully for NLOS identification in localisation applications.

6 Conclusions

We presented a statistical decision-theoretic approach to NLOS identification based on TOA, RSS and RMS delay spread estimates. Based on the parameters from extensive measurement results, we characterised the ability of TOA, RSS and RMS delay-spread estimates to distinguish between LOS and NLOS propagation. We showed that although utilising all three estimates jointly in detecting the nature of propagation yields the best results in the presence of accurate distance information, the RMS delay-spread estimate is the best indicator of the nature of propagation when perfect distance information is not available. Our results suggest that hypothesis-testing of the RMS delay-spread estimates of UWB signals can serve as a robust and computationally efficient means of identifying NLOS propagation, and does not require distance information or considerable statistical information. The efficacy of hypothesis testing of the RMS delay spread was demonstrated in a location-tracking experiment with indoor UWB measurements, where we showed that utilising the RMS delay spread for NLOS identification results in negligible degradation in localisation accuracy when compared to the case with perfect channel state information.

7 References

- Win, M.Z., and Scholtz, R.A.: ‘Impulse radio: How it works’, *IEEE Commun. Lett.*, 1998, 2, pp. 36–38
- Molisch, A.F., Balakrishnan, K., Cassioli, D. *et al.*: ‘IEEE 802.15.4a channel model-final report’. Technical Report, IEEE 802.15-04-0662-01-04a, September 2004
- Lee, J.-Y., and Scholtz, R.A.: ‘Ranging in a dense multipath environment using an UWB radio link’, *IEEE J. Selected Areas Commun.*, 2000, 20, pp. 1677–1683
- Oppermann, I., Stoica, L., Rabbachin, A., Shelby, Z., and Haapola, J.: ‘UWB wireless sensor networks: UWEN – a practical example’, *IEEE Commun. Mag.*, 2004, 42, pp. S27–S32
- Qi, Y., Kobayashi, H., and Suda, H.: ‘Analysis of wireless geolocation in a non-line-of-sight environment’, *IEEE Trans. Wirel. Commun.*, 2006, 5, pp. 672–681

- 6 Wylie, M.P., and Holtzman, J.: 'The non-line of sight problem in mobile location estimation'. 5th IEEE Int. Conf. on Universal Personal Communications, 1996, vol. 2, pp. 827–831
- 7 Kull, B., and Zeisberg, S.: 'UWB receiver performance comparison'. 2004 Int. Workshop on Ultra Wideband Systems, 18–21 May 2004, pp. 21–25
- 8 Venkatesh, S., and Buehrer, R.M.: 'A linear programming approach to NLOS error mitigation in sensor networks'. Proc. Fifth Int. Conf. on Information Processing in Sensor Networks (IPSN '06), April 2006, vol. 1, pp. 301–308
- 9 Venkatesh, S., and Buehrer, R.M.: 'NLOS mitigation using linear programming in ultra-wideband location-aware networks', *IEEE Trans. Veh. Technol.*, November 2007, To be published
- 10 Borrás, J., Hatrack, P., and Mandayam, N.B.: 'Decision theoretic framework for NLOS identification'. 1998 Vehicular Technology Conf., (VTC98), May 1998, vol. 2, pp. 1583–1587
- 11 Buehrer, R., Davis, W., Safaai-Jazi, A., and Sweeney, D.: 'Ultra-wideband propagation measurements and modeling – DARPA NETEX final report'. Technical Report, January 2004, Virginia Tech. Available at http://www.mprg.org/people/buehrer/ultra/darpa_netex.shtml
- 12 Ghassemzadeh, S.S., Jana, R., Rice, C.W., Turin, W., and Tarokh, V.: 'Measurement and modeling of an ultra-wide bandwidth indoor channel', *IEEE Trans. Commun.*, 2004, **52**, pp. 1786–1796
- 13 Denis, B., Keignart, J., and Daniele, N.: 'Impact of NLOS propagation upon ranging precision in UWB systems'. 2003 IEEE Conf. on Ultra Wideband Systems and Technologies, Nov 2003, pp. 379–383
- 14 Zhang, J.R., Kennedy, R.A., and Abhayapala, T.D.: 'Cramer-Rao lower bounds for the time delay estimation of UWB signals'. 2004 IEEE Int. Conf. on Communications, June 2004, vol. 6, pp. 3424–3428
- 15 Irahhtauten, Z., Nikookar, H., and Janssen, G.J.: 'An overview of ultra wide band indoor channel measurements and modeling', *IEEE Microw. Wirel. Compon. Lett.*, 2004, **14**, pp. 386–388
- 16 Cramer, J.-M., Win, M.Z., and Scholtz, R.A.: 'Evaluation of the multipath characteristics of the impulse radio channel'. The Ninth IEEE Int. Symp. on Personal Indoor and Mobile Radio Communications, 1998, vol. 2, pp. 864–868
- 17 Yano, S.M.: 'Investigating the ultra-wideband indoor wireless channel'. IEEE VTS 55th Vehicular Technology Conf, October 2002, vol. 3, pp. 1200–1204
- 18 Ghassemzadeh, S., Greenstein, L., Sveinsson, T., Kavcic, A., and Tarokh, V.: 'UWB delay profile models for residential and commercial indoor environments', *IEEE Trans. Veh. Technol.*, 2005, **54**, pp. 1235–1244
- 19 Kay, S.M.: 'Fundamentals of statistical processing, volume I: estimation theory' (Prentice-Hall Inc., 1993, 2nd edn.)
- 20 Chong, C.-C., Kim, Y., and Lee, S.: 'Channel model parameterization of the indoor residential environment'. Technical Report, submitted to IEEE P802.15 Working Group for Wireless Personal Area Networks (WPANs), July 2004, available at: <http://grouper.ieee.org/groups/802/15/pub/2004/July04/>
- 21 Foerster, J.: 'Channel modeling sub-committee Report Final (Doc: IEEE 802-15-02/490r1-SG3a)'. Technical Report, February 2002, Available at <http://grouper.ieee.org/groups/802/15/pub/2002/Nov02/>
- 22 Guvenc, I., and Sahinoglu, Z.: 'Threshold selection for UWB TOA estimation based on kurtosis analysis', *IEEE Commun. Lett.*, 2005, **9**, pp. 1025–1027
- 23 Ghassemzadeh, S.S., Greenstein, L.J., Kavcic, A., Sveinsson, T., and Tarokh, V.: 'UWB indoor delay profile model for residential and commercial environments'. 2003 IEEE Vehicular Technology Conf. (VTC 2003-Fall), October 2003, vol. 5, pp. 3120–3125
- 24 Chong, C.-C., Kim, Y.-E., Yong, S.K., and Lee, S.-S.: 'Statistical characterisation of the UWB propagation channel in indoor residential environment', *IEEE Trans. Commun.*, 2005, **5**, pp. 503–512

8 Appendix 1: Distribution of $\hat{\tau}_0$ under NLOS conditions

Under NLOS propagation conditions, the TOA estimate is modelled as

$$\hat{\tau}_0 = \frac{d}{c} + n_\tau + b_\tau, H = H_1$$

where n_τ is a zero-mean Gaussian random variable with variance σ_τ^2 and b_τ is exponentially distributed with mean

λ_b . Therefore the probability density function of $\hat{\tau}_0$ is defined by a convolution of the density functions of n_τ and b_τ

$$\begin{aligned} f_{\hat{\tau}_0}(\tau, d|H_1) &= (2\pi\lambda_b^2\sigma_\tau^2)^{-1/2} \\ &\int_0^\infty \exp\left(-\frac{(\tau - (d/c) - b)^2}{2\sigma_\tau^2}\right) \times \exp\left(-\frac{b}{\lambda_b}\right) db, \\ &= (\pi\lambda_b^2)^{-1/2} \int_{-\infty}^{\tau - (d/c)/\sqrt{2}\sigma_\tau} \exp(-y^2) \\ &\quad \times \exp\left(-\frac{\tau - (d/c) - \sqrt{2}\sigma_\tau y}{\lambda_b}\right) dy \\ &= (\pi\lambda_b^2)^{-1/2} \exp\left(\frac{\sigma_\tau^2}{2\lambda_b^2}\right) \exp\left(-\frac{\tau - (d/c)}{\lambda_b}\right) \\ &\quad \times \int_{-\infty}^{\tau - (d/c)/\sqrt{2}\sigma_\tau} \exp\left(-\left(y - \frac{\sigma_\tau}{\sqrt{2}\lambda_b}\right)^2\right) dy \\ &= \frac{1}{2\lambda_b} \exp\left(\frac{\sigma_\tau^2}{2\lambda_b^2}\right) \exp\left(-\frac{\tau - (d/c)}{\lambda_b}\right) \\ &\quad \times \left[1 + \operatorname{erf}\left(\frac{\lambda_b(\tau - (d/c)) - \sigma_\tau^2}{\sqrt{2}\sigma_\tau\lambda_b}\right)\right] \end{aligned}$$

where $\operatorname{erf}(x) = (2/\sqrt{\pi}) \int_0^x e^{-y^2} dy$.

9 Appendix 2: Derivation of P_e^* and T^* for positive, Gaussian RDS estimates

The probability density functions of the RDS estimates in LOS and NLOS scenarios are modelled as positive (truncated) Gaussian density functions

$$f(x) = \begin{cases} \frac{1}{Q(-\mu_L/\sigma_L)} \cdot \frac{1}{\sqrt{2\pi\sigma_L^2}} e^{-(x-\mu_L)^2/2\sigma_L^2} u(x), & H = H_0 \\ \frac{1}{Q(-\mu_N/\sigma_N)} \cdot \frac{1}{\sqrt{2\pi\sigma_N^2}} e^{-(x-\mu_N)^2/2\sigma_N^2} u(x), & H = H_1 \end{cases} \quad (10)$$

where $Q(x) = 1/\sqrt{2\pi} \int_x^\infty e^{-x^2/2} dx$, and $u(x)$ is the Heaviside function. The means μ_L , μ_N and the standard deviations σ_L , σ_N are specified in Table 2. Let the threshold selected for differentiating between LOS and NLOS RDS estimates be T . For a given sample RDS measurement Z , the probability of error in the detection of the nature of the channel is given by

$$P_e(T) = p_L \cdot \Pr\{Z \geq T|H_0\} + p_N \cdot \Pr\{Z < T|H_1\} \quad (11)$$

It must be pointed out for a given *ad hoc* indoor scenario, the probability p_L that a given link between two nodes is LOS is not necessarily equal to the probability p_N that the link is NLOS. In the absence of a priori

knowledge, we assume $p_L = p_N = 1/2$. From (10) and (11), we obtain

$$P_e(T) = p_L \cdot \frac{Q((T - \mu_L)/\sigma_L)}{Q(-\mu_L/\sigma_L)} + p_N \cdot \left(1 - \frac{Q((T - \mu_N)/\sigma_N)}{Q(-\mu_N/\sigma_N)}\right)$$

To find the optimal threshold T^* that minimises the probability of error, we set $(d/dT)P_e|_{T=T^*} = 0$, and it is straightforward to show that T^* is the solution of the

quadratic equation

$$T^{*2} \left(\frac{1}{\sigma_L^2} - \frac{1}{\sigma_N^2} \right) + 2T^* \left(\frac{\mu_N}{\sigma_N} - \frac{\mu_L}{\sigma_L} \right) + \frac{\mu_L^2}{\sigma_L^2} - \frac{\mu_N^2}{\sigma_N^2} = 2 \log \left(\frac{p_L \sigma_N Q(-\mu_N/\sigma_N)}{p_N \sigma_L Q(-\mu_L/\sigma_L)} \right) \quad (12)$$

Then, minimum probability of channel detection error is given by $P_e^* = P_e(T^*)$.